Available online at www.sciencedirect.com

ScienceDirect

Energy Procedia 60 (2014) 13 – 22

Energy Procedia

E-MRS Spring Meeting 2014 Symposium Y "Advanced materials and characterization techniques for solar cells II", 26-30 May 2014, Lille, France

ITO-free anode with plasmonic silver nanoparticles for high efficient polymer solar cells

Pasquale Morvillo*, Anna De Girolamo Del Mauro, Giuseppe Nenna,

Rosita Diana, Rosa Ricciardi, Carla Minarini

ENEA, UTTP-NANO, Piazzale E. Fermi 1, 80055 Portici, Italy

Abstract

In this work we improved the performance of ITO-free polymer solar cells (PSCs) by incorporating silver nanoparticles (AgNPs) in the highly conductive (HC) PEDOT:PSS anode. The AgNPs were synthetized *in-situ* in the PEDOT:PSS water dispersion. This anode was used to realize PSCs with the following geometry: glass/HC-PEDOT:PSS/PEDOT:PSS/PBDTTT-C:[70]PCBM/Ca/Al. All the devices were characterized by UV-VIS spectroscopy, impedance spectroscopy, IV light, IV dark and quantum efficiency measurements. The presence of AgNPs in the HC-PEDOT:PSS anode contributes to improve the absorption of the photoactive layer and to lower the resistivity of the anode.

Peer-review under responsibility of The European Materials Research Society (E-MRS)

Keywords: polymer solar cells, silver nanoparticles, plasmonic effect, impedance spectroscopy, ITO-free.

1. Introduction

Polymer solar cells (PSCs) are a promising alternative to silicon-based devices because they have several advantages like the good flexibility, the light-weight and the low-cost manufacturing that can be reached by roll-to-

* Corresponding author. Tel.: +39 081 7723260; fax: +39 081 7723344.
E-mail address: pasquale.movillo@enea.it

Peer-review under responsibility of The European Materials Research Society (E-MRS)
doi:10.1016/j.egypro.2014.12.336

roll printing and coating techniques [1-4]. Recently, power conversion efficiency (PCE) surpassing 9% has been reported [5]. The most successful device configuration is based on the bulk heterojunction (BHJ) concept where an interpenetrating network, with nanometer phase separation, of electron donor and acceptor materials is placed between two contact with different work function [6, 7]. However, the PCE of these devices need to be enhanced even more before PSCs can be commercially viable. One of the main limits of the PCE is the insufficient light absorption due to the narrow absorption range of the photoactive materials and the ultrathin film thickness. A promising approach used to improve this bottleneck is the introduction of metallic nanoparticles (NPs) inside the layers of the PSCs in order to increase the light harvesting and the PCE of the devices. This enhancement is mainly due to the plasmonic effects of these NPs ascribed to near-field enhancement and light-scattering [8].

In the most used device configuration, indium tin oxide (ITO) is used as transparent conducting anode but it is not desirable for PSCs fabrication for the increasing cost of indium [9], the limited mechanical flexibility and the patterning that involves a lot of chemicals. Recently, poly(3,4-ethylenedioxythiophene):poly(styrene sulfonate) (PEDOT:PSS) polymer has been investigated as innovative material for replacing ITO due to its high transparency in the visible region, long-term stability and solution process ability [10, 11].

In this work, we improved the performance of ITO-free PSCs by incorporating silver nanoparticles (AgNPs) in the highly conductive PEDOT:PSS anode. The AgNPs were synthetized *in-situ* in the PEDOT:PSS water dispersion. This anode was used to realize PSCs with the following geometry: glass/HC-PEDOT:PSS/PEDOT:PSS/active layer/Ca/Al). The active layer was a blend of poly[(4,8-bis-(2-ethylhexyloxy)-benzo[1,2-b;4,5-b']dithiophene)-2,6-diyl-alt-(4-(2-ethylhexanoyl)-thieno[3,4-b]thiopene)-2,6-diyl] (PBDTTT-C) and [6,6]-phenyl C_{71} butyric acid methyl ester ([70]PCBM). When PBDTTT-C is used as donor material in conventional PSCs, PCE up to 6% has been reached [12]. All the devices were characterized by UV-Vis spectroscopy, impedance spectroscopy (IS), IV light, IV dark and external quantum efficiency (EQE) measurements. We made a comparative study of the electrical behavior of different PSCs in order to investigate the influence of AgNPs on the absorption of the photoactive layer and on the resistivity of the anode.

2. Experimental

2.1. Materials

To realize ITO-free PSC devices the following materials were used as received: Corning® Eagle XG 1 mm thick boro-aluminosilicate glass substrate (Delta Technologies, LTD), Clevios™ PH 1000 and Clevios P AI4083 PEDOT:PSS aqueous dispersions (Heraeus Precious Metals GmbH), dimethyl sulfoxide (Sigma-Aldrich Co.), $AgNO_3$ (≥ 99.5%) (Sigma-Aldrich Co.), $NaBH_4$ (≥99%) (Sigma-Aldrich Co.), PBDTTT-C (Solarmer), [70]PCBM (Solenne BV), anhydrous 1,2-dichlorobenzene (Sigma-Aldrich Co.), diiodooctane (DIO) (Sigma-Aldrich Co.), Calcium (Sigma-Aldrich Co.), Aluminum (Kurt J. Lesker). Blend of donor: acceptor was prepared prior to device fabrication. PBDTTT-C:[70]PCBM solution (ratio 1 : 1.5) was obtained, inside a nitrogen glove-box, by dissolving both components in 1,2-dichlorobenzene with an initial donor concentration of 15 mg/ml. The solution was left stirring overnight at 40 °C. After 24 h the corresponding amount of DIO (3% v/v) was added. The new solution was stirred 1 h at 70 °C just before film deposition. Moreover, before realization of devices, the highly conductive polymer dispersion used as anode was prepared by doping with dimethyl sulfoxide (DMSO) (5% v/v) the commercial aqueous PEDOT:PSS dispersion (HC-PEDOT:PSS) [13].

2.2. AgNPs synthesis

Silver nanoparticles (AgNPs) were synthesized directly into the HC-PEDOT:PSS aqueous dispersion (in situ preparation) by chemical reduction of Ag^+ of silver nitrate ($AgNO_3$) to Ag^0 using as reducing agent sodium borohydride ($NaBH_4$). 15 mL of HC-PEDOT:PSS aqueous dispersion was added to 1 mL of a 29.4 mM deionized water solution of $AgNO_3$ (5 mg) under vigorous magnetic stirring at room temperature. Then, 2 mL of 52.9 mM (4 mg) deionized water $NaBH_4$ solution was added drop-wise. After the addition of the reducing agent, the reaction

mixture showed a color change from navy blue to yellowish brown (Fig. 1). The color change indicates the formation of silver nanoparticles [14].

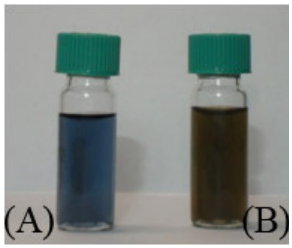

Fig. 1. Photograph of the dispersions of HC-PEDOT:PSS (A) and HC-PEDOT:PSS with AgNPs (B).

2.3. Device Realization

Devices were fabricated in the configuration Glass/HC-PEDOT:PSS (with or without AgNPs)/PEDOT:PSS/Active layer/Ca/Al (Fig. 2). Glass substrates were first cleaned in subsequent detergent, acetone and isopropyl alcohol ultrasonic baths then dried in an oven at 150°C under vacuum. After cleaning, the substrates were treated with UV-ozone to improve the wettability of the PEDOT:PSS aqueous solution. After filtration through a 0.45 μm polyvinyl difluoride (PVDF) filter, the HC-PEDOT:PSS (PH 1000 doped with DMSO) suspensions with and without AgNPs were deposited by spin-coating onto 2.5 × 2.5 cm^2 glass substrates and annealed at 140 °C overnight. The obtained ITO-free anodes are 150 nm (HC-PEDOT:PSS) and 120 nm (HC-PEDOT:PSS+AgNPs) thick. The polymeric anode layer was suitably patterned by removing a part of the film to avoid short circuit after cathode deposition.

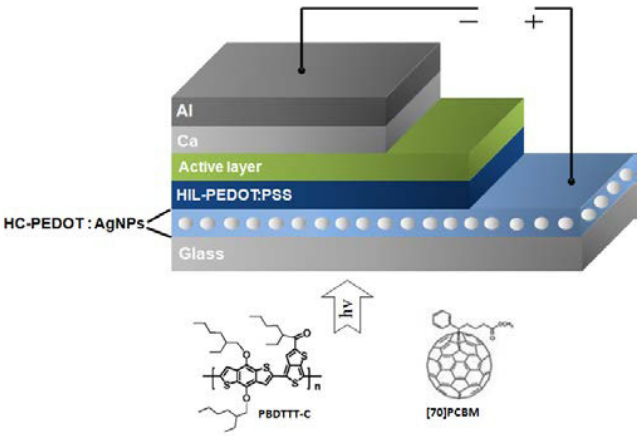

Fig. 2. Device architecture of the investigated polymer solar cells and the chemical structures of the materials used as active layer: PBDTTT-C and [70]PCBM.

A 40nm thick PEDOT:PSS anode buffer layer was spin-cast on the top of glass/HC-PEDOT:PSS (reference device) or glass/HC-PEDOT:PSS containing AgNPs, then dried in a vacuum oven at 150°C for 1 h. The active layer (80 nm) was prepared by dissolving PBDTTT-C (15 mg/ml) and [70]PCBM (22.5 mg/ml) in a mixed solvent of 1,2dichlorobenzene/1,8-diiodoctane (97:3% by volume) and spin coated on the top of PEDOT:PSS. The Ca electrode (20 nm) capped with Al (100 nm) was deposited on the active layer by thermal evaporation in ultra-high vacuum (10^{-7} mbar) using a shadow mask to define the active area of the device (20 mm^2).

2.4. Characterizations

2.4.1. Single Layers

The film thicknesses and the roughness were measured by KLA Tencor P-10 surface profiler. UV–Vis optical transmittance analysis of layers deposited on glass substrates and of suspensions were carried out by using Perkin-Elmer Lambda 900 spectrophotometer. The surface morphology of HC-PEDOT:PSS films with and without AgNPs were analyzed by scanning electron microscopy (SEM). The electrical conductivity of the films was evaluated from sheet-resistance measurements by means of a four-point probe system (Napson Co.). The particle size distribution measurements were performed by means of a dynamic light scattering (DLS) system (HPPS 3.1, Malvern Instruments).

2.4.2. Devices

All the PSC were characterized in air and without encapsulation by means of EQE and IV measurements performed in the dark and under simulated AM 1.5G illumination (100 mW/cm^2). IV light characteristic was measured with a Keithley 2400 source measure unit (Keithley Instruments Inc., Cleveland, USA). The voltage ramp rate, controlled by a PC program, was of 10 mV/s from positive to negative potential. Simulated AM 1.5G white light illumination was provided by a class "AAA" Wacom Solar Simulator, Model WXS155S, equipped with two lamps (Xenon and Halogen) and its intensity was calibrated using a filtered mono-Si reference cell (certified by ESTI) for 1 sunlight intensity of 100 mW/cm^2. All the photovoltaic properties were recorded in ambient air at room temperature (~25 °C). Alternate current measurements, applying an amplitude voltage of 0.1 V, have been performed by using an HP 4192 A. The frequency range investigated was $10^2 \div 10^7$ Hz.

3. Results and Discussion

3.1 HC-PEDOT:PSS with AgNPs layer

Fig. 3 reports the SEM image of the HC-PEDOT:PSS with AgNPs film deposited on glass substrate and the particle size distribution of the AgNPs in the HC-PEDOT:PSS suspension. The SEM study analysis of HC-PEDOT:PSS film containing silver nanoparticles showed that the AgNPs are roughly spherical and uniformly distributed in PEDOT:PSS layer.

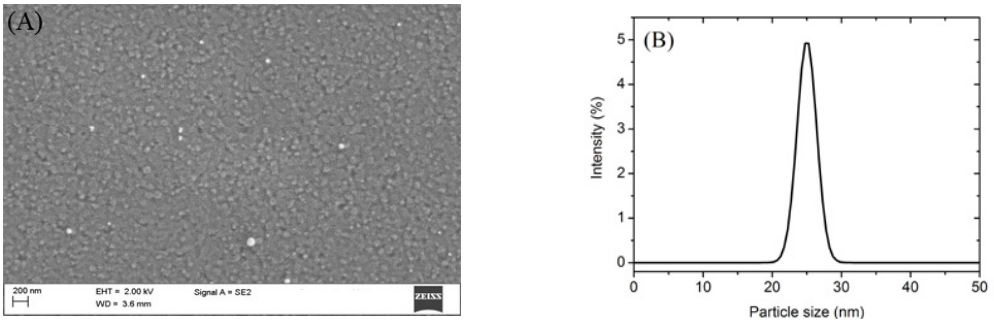

Fig.3. SEM image of HC-PEDOT:PSS film with AgNPs (white dots) (A) and Particle Size Distribution of AgNPs in HC-PEDOT:PSS aqueous dispersion (B).

The particle average sizes of the primary Ag grains are nearly 25 nm in diameter, which is in good agreement with the value observed by DLS analysis (Fig. 3B). Moreover, no apparent aggregation is observed in the film.

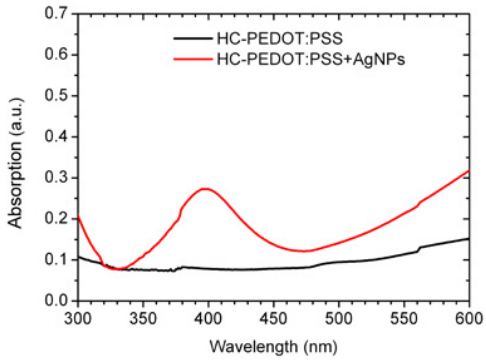

Fig. 4. UV-Vis absorption spectra of HC-PEDOT:PSS and HC-PEDOT:PSS with AgNPs suspensions.

In Fig. 4 the absorption spectra of pristine HC-PEDOT:PSS and HC-PEDOT:PSS with AgNPs suspensions are compared. The HC-PEDOT:PSS water suspension with AgNPs exhibits a strong absorption peak at nearly 400nm, which is characteristic of the surface plasmon band for silver spherical nanoparticles [15]. In the absorption curve of HC-PEDOT:PSS with AgNPs film (not shown), the plasmon peak is also present and it shifts to 435 nm.

In Fig. 5 the transmittance spectra of pristine HC-PEDOT:PSS with and without AgNPs films are compared. Both films appear highly transparent (trasmittance value $\approx$ 83%) in the visible range. The transmission spectrum of the HC-PEDOT:PSS with AgNPs film (Fig. 5) shows a slightly decrease in the region between 400 and 500 nm which is indicative of surface plasmon absorption by metal NPs. At wavelength greater than 550nm, the transmittance of the HC-PEDOT:PSS+AgNPs film is greater due to the lower thickness of this film (120 nm vs 150 nm for the pristine HC-PEDOT:PSS film).

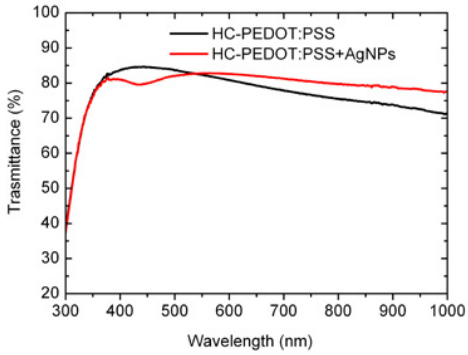

Fig. 5. Trasmittance spectra of the pristine HC-PEDOT:PSS and HC-PEDOT:PSS with AgNPs films deposited on glass substrate.

In Fig. 6 the X-ray diffraction patterns of HC-PEDOT:PSS with and without AgNPs films deposited on glass are reported. The comparison of the two profiles confirms the formation of silver in the HC-PEDOT:PSS suspension by *in situ* preparation. In fact, the film obtained by spin coating of HC-PEDOT:PSS dispersion submitted to the *in situ* synthesis of AgNPs presents diffraction peaks at 2θ of 38.2°, 44°, 64° and 78° that could be indexed as (111), (200), (220) and (311) Bragg's reflections of the face-centred cubic (fcc) structure of silver (JCPDS file No. 04-0783).

The main properties of HC-PEDOT:PSS and HC-PEDOT:PSS containing AgNPs thin films are reported in Table 1.

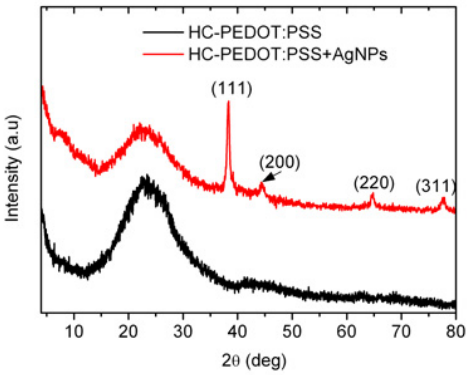

Fig. 6. X-Ray diffraction patterns of HC-PEDOT:PSS films with and without AgNPs deposed on glass substrates.

Table 1. Summary of properties of HC-PEDOT:PSS and HC-PEDOT:PSS containing AgNPs thin films.

Films	Thickness (nm)	Roughness (Rq) (nm)	Waviness (nm)	Sheet Resistance (Ω /□)	σ (S/cm)
HC-PEDOT:PSS	150	1.9	3	93	714
HC-PEDOT:PSS + AgNPs	120	3.7	19	108	770

3.2 Polymer Solar cells

PSC devices using HC-PEDOT:PSS (anode) with and without AgNPs were realized under an inert nitrogen atmosphere and characterized in air, without encapsulation, by EQE and IV measurements performed in the dark and under simulated AM 1.5 G illumination (100 mW/cm^2). Fig. 7 shows the IV light curves of both kinds of device.

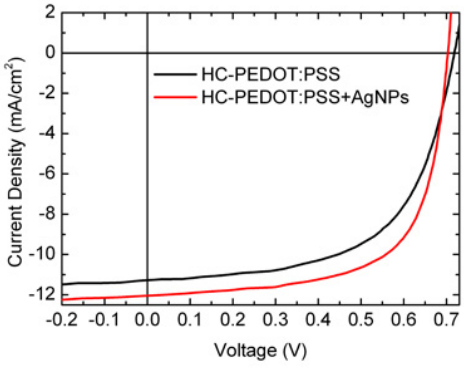

Fig. 7. I-V light curves measured at 25°C under simulated AM1.5G conditions (100mW/cm^2), of PBDTTT-C:[70]PCBM polymer solar cells having as anode: HC-PEDOT:PSS (black line) and HC-PEDOT:PSS+AgNPs (red line).

In Table 2, the corresponding PCE, open circuit voltage (V_{oc}), short circuit current density (J_{sc}), fill factor (FF), series resistance (R_s) and shunt resistance (R_{sh}) are reported. The PCE of the HC-PEDOT:PSS-based device is 4.8% while the HC-PEDOT:PSS+AgNPs one reaches 5.6%. The J_{sc} is higher for the HC-PEDOT:PSS+AgNPs-based device (12.1 vs 11.3 mA/cm^2 for the device without AgNPs). The decrease of the V_{oc} for the device having the HC-

PEDOT:PSS+AgNPS anode, is due to the higher recombination rate at the interface for the presence of metal nanoparticles in the anode that can act as traps for the charge carriers.

Table 2: Photovoltaic properties of polymer solar cells having HC-PEDOT:PSS and HC-PEDOT:PSS+AgNPs anode.

Anode	PCE (%)	Jsc (mA/cm^2)	Voc (mV)	FF (%)	Rs (Ωcm^2)	Rsh (Ωcm^2)
HC-PEDOT:PSS	4.83	11.3	719	60	9	855
HC-PEDOT:PSS + AgNPs	5.60	12.1	703	66	5	882

The IV dark curves of both kind of devices are reported in Fig. 8. In dark environment, both cells show similar behavior in forward voltage, while in reverse the device with HC-PEDOT:PSS+AgNPs has a lower current density: this is in agreement with the higher R_{sh} of this device under illumination (Table 2). The EQE of the ITO-free devices is reported in Fig. 9. Both cells show a broad response range from 300 to 900 nm, with values greater than 45% (HC-PEDOT:PSS anode) and 50% (HC-PEDOT:PSS+AgNPs anode) in the visible range. The response of the device with AgNPs is greater than that of the reference device confirming the trend of the current outputs of the corresponding IV-light curves. This enhancement is due to the plasmonic effect of the AgNPs (in the region between 400-500nm), due to near-field enhancement or light scattering, and the better transmittance of the anode (for wavelength greater than 550nm).

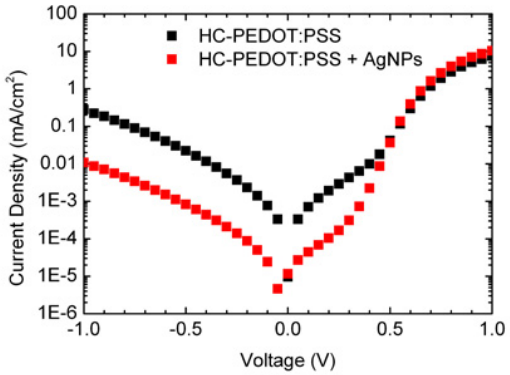

Fig. 8. I-V dark curves measured at 25°C of PBDTTT-C:[70]PCBM solar cells having as anode: HC-PEDOT:PSS (■) and HC-PEDOT:PSS+AgNPs (■).

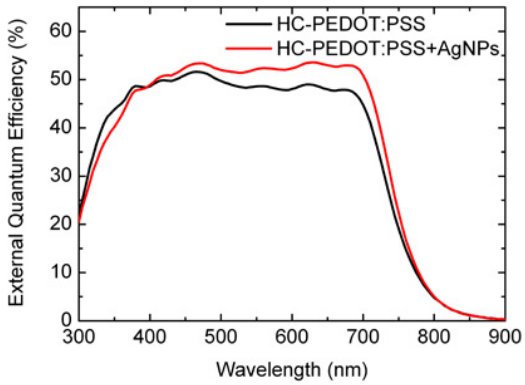

Fig. 9. External Quantum Efficiency of PBDTTT-C: [70]PCBM solar cells having as anode: HC-PEDOT:PSS (black line) and HC-PEDOT:PSS+AgNPs (red line).

In order to investigate the charge injection across the organic–organic interfaces, the effects of the charge injection rate and the contact resistances introduced by the different anodes on the device performances were investigated through the device operation in dynamic regime.

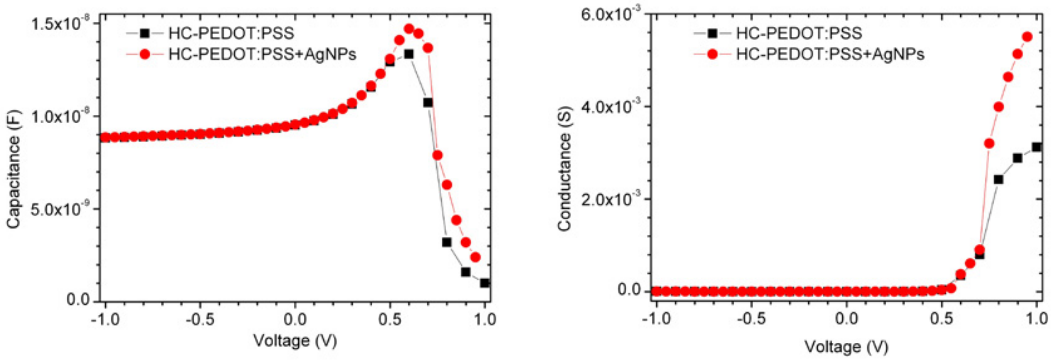

Fig. 10. Capacitance and Conductance vs Voltage of PSCs at fixed frequency (1 KHz) of PBDTTT-C:[70]PCBM solar cells having as anode: HC-PEDOT:PSS (■) and HC-PEDOT:PSS+AgNPs (●).

In Fig.10 the capacitance and the conductance versus voltage of PSCs at fixed frequency (1 KHz) are reported. Black curves are related to the reference cells, without the addition of AgNPs. The Capacitance peak reveals that there is no appreciable change in the V_{on} of the devices while the conductance plot confirms the results obtained with the IV curves.

The conductance analysis of the device with the doped and undoped HC-PEDOT:PSS anode exhibited a saturation effect in both curves but it seems to be stronger in the device without the AgNPs due to a higher shunt resistance [16] and, as consequence, to an higher contact resistance.

In the impedance spectroscopy (IS) experiment, an alternating electrical signal $v(t) = V_{AC}*sin(2\pi f*t)$ with small amplitude V=0.1 V and frequency (f) values from 100 Hz to 10^7 Hz was applied and in Fig. 11 dielectric loss and capacitance versus 2*π*frequency of PSCs were reported.

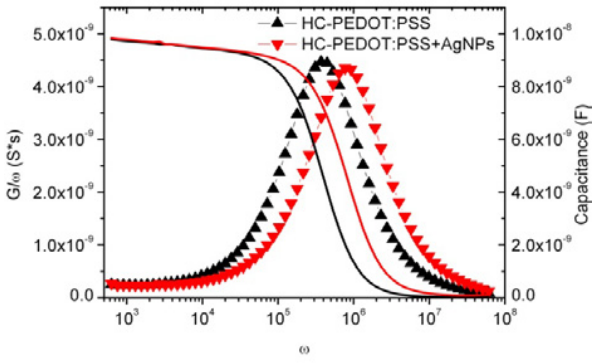

Fig. 11. Dielectric loss and Capacitance vs ω = 2*π*Frequency of PBDTTT-C:[70]PCBM solar cells having as anode: HC-PEDOT:PSS (▲) and HC-PEDOT:PSS+AgNPs (▼).

The change in the cut-off and the relative shift to higher frequency reveal the lowering of the contact resistance by doping the HC-PEDOT with AgNPs [17]. In general, the injection process is provided by the kinetics of filling and releasing of the states at metal–organic interface [18] and organic–organic interface [19] and, in particular, at the interface between anode or HIL (hole injection layer) and HTL (hole transport layer) which can be modified whether doping the electrode materials or applying surface treatments to the electrode contact [20,21]. The change in the contact resistance causes also a change in the complementary quantity of the capacitance, the dielectric loss (the conductance G divided by the angular frequency ω) [13], whose peak showed the same frequency shift. According with the conductance method we can obtain the interface trap level distribution (D_{it}) and in particular using:

$$D_{it} = \frac{G/\omega_{max}}{0.402eS}$$

We can observe that this time D_{it} is lower for the HC-PEDOT:PSS because of the lowering in the $(G/\omega))_{max}$ and the same tendency follow the time constant (τ) (the reverse of ω at G/ω peak) for the trap-detrapping charges. All these phenomena give us enough information about the drastic modification of the interfacial interaction between the anode electrode and the overlying organic materials because of the addition of AgNPs in the HC-PEDOT:PSS layer. The reduction in the number of D_{it} probably reflects a higher reorganization and optimization of the interface states. On the other hand the lowering of τ justifies once again the best performance of the conductance as a function of the voltage that we also had observed in Fig. 10. All these aspects give us understanding about the addition of AgNPs in HC-PEDOT:PSS anode that drastically changes not only the optical performances of the devices but also and especially the electric ones and that this type of situations have to be analyzed with extreme caution and with different points of view in terms of experimental analysis.

4. Conclusions

In this work we improved the performance of ITO-free polymer solar cells (PSCs) by incorporating silver nanoparticles (AgNPs) in the highly conductive (HC) PEDOT:PSS anode. We realized ITO-free PSCs using HC-PEDOT:PSS anodes with and without AgNPs. The device incorporating NPs shows superior performance compared to the reference one. The presence of the AgNPs in the HC-PEDOT:PSS anode contributes to improve the absorption of the photoactive layer and to lower the resistivity of the anode.

Acknowledgements

This work has been financially supported by the Italian Ministry of Education, University and Research(MIUR) through the National Project entitled Relight (PN: PON02 00556 3306937).

References

[1] Krebs F C. Fabrication and processing of polymer solar cells: A review of printing and coating techniques. Sol. Energy Mater. Sol. Cells 2009; 93:394–412.
[2] Krebs F C. Roll-to-roll fabrication of monolithic large-area polymer solar cells free from indium-tin-oxide. Sol. Energy Mater. Sol. Cells 2009; 93:1636–41.

[3] Galagan V, de Vries I, Langen A, Andriessen R, Verhees W, Veenstra S, Kroon J. Technology development for roll-to-roll production of organic photovoltaics. Chem. Eng. Process, in press.
[4] Morvillo P, Diana R, Fontanesi C, Ricciardi R, Lanzi M, Mucci A, Tassinari F, Schenetti L, Minarini C, Parenti F. Low band gap polymers for application in solar cells: synthesis and characterization of thienothiophene–thiophene copolymers. Polym. Chem. 2014;5:2391-400.
[5] He Z, Zhong C, Su S, Xu M, Wu H, Cao Y. Enhanced power-conversion efficiency in polymer solar cells using an inverted device structure. Nature Photonics 2012;6(9):591-5.
[6] Yu G, Heeger A J. Charge separation and photovoltaic conversion in polymer composites with internal donor/acceptor heterojunctions. Journal of Applied Physics 1995; 78:4510-15.
[7] Yu G, Gao J, Hummelen J C, Wudl F, Heeger A J. Polymer Photovoltaic Cells: Enhanced Efficiencies via a Network of Internal Donor-Acceptor Heterojunctions. Science 1995; 270:1789-91.
[8] a) Lu L, Luo Z, Xu T, Yu L. Cooperative Plasmonic Effect of Ag and Au Nanoparticles on Enhancing Performance of Polymer Solar Cells. Nano Letters 2012;13:59-64. b)Wang D H, Kim D Y, Choi K W, Seo J H, Im S H, Park J H, Park O O, Heeger A J. Enhancement of Donor–Acceptor Polymer Bulk Heterojunction Solar Cell Power Conversion Efficiencies by Addition of Au Nanoparticles. Angew. Chem., Int. Ed. 2011;50:5519-23.
[9] Krebs F C, Tromholt T, Jorgensen M. Upscaling of polymer solar cell fabrication using full roll-to-roll processing. Nanoscale 2010;2: 873–86.
[10] Winther-Jensen B, Krebs F C. High-conductivity large-area semi-transparent electrodes for polymer photovoltaics by silk screen printing and vapour- phase deposition. Sol. Energy Mater. Sol. Cells 2006; 90: 123–32.
[11] Ahlswede E, Muhleisen W, Wahi M W b M, Hanisch J, Powalla M. Highly efficient organic solar cells with printable low-cost transparent contacts. Appl. Phys. Lett. 2008; 92: 143307-14.
[12] He Z C, Zhong C M, Huang X, Wong W Y, Wu H B, Chen L W, Su S J, Cao Y. Simultaneous enhancement of open-circuit voltage, short-circuit current density and fill factor in polymer solar cells. Adv. Mater. 2011; 23:4636-43..
[13] De Girolamo Del Mauro A, Nenna G, Villani F, Minarini C. Study of the effect of the doped poly(3,4-ethylenedioxythiophene):poly(styrene sulfonate) polymeric anode on the organic light-emitting diode performances. Thin Solid Films 2012;520:5386–91.
[14] Jin R, Cao Y W, Mirkin C A, Kelly K L, Schatz G C, Zheng J G. Photoinduced conversion of silver nanospheres to nanoprisms. Science 2001; 294:1901-03.
[15] Ghosh S, Rasmusson J, Inganas O. Supramolecular self-assembly for enhanced conductivity in conjugated polymer blends: Ionic crosslinking in blends of poly(3,4-ethylenedioxythiophene)-poly(styrenesulfonate) and poly(vinylpyrrolidone). Adv. Mater. 1998;10:1097-99.
[16] Aubry V, Meyer F J. Schottky diodes with high series resistance: Limitations of forward I-V methods. Appl. Phys. 1994: 76:7973-84.
[17] Nowy S, Ren W, Wagner J, Weber J A, Brutting Wolfgang. Impedance spectroscopy of organic hetero-layer OLEDs as a probe for charge carrier injection and device degradation. Proc. of SPIE 2009;7415:74150G1-12.
[18] Garcia-Belmonte G, Bisquert J, Bueno P R, Graeff C F O, Castro F A. Kinetics of interface state-limited hole injection in α-naphthylphenylbiphenyl diamine (α-NPD) thin layers Synth. Met. 2009;159:480-86.
[19] Arkhipov V I, Emelianova E V, Bassler H J. Charge carrier transport and recombination at the interface between disordered organic dielectrics.Appl. Phys. 2001; 90:2352-56.
[20] De Girolamo Del Mauro A., Nenna G, Bizzarro V, Grimaldi I A,Villani F, Minarini C J. Analysis of the Performances of Organic Light-Emitting Devices with a Doped or an Undoped Polyaniline–Poly(4-styrenesulfonate) Hole-Injection Layer.Appl. Polym. Sci. 2011; 122: 3618-22.
[21] Serpengüzel A, Badenes G, Righini G C. Photonic Materials, Devices, and Applications II, Proceeding of SPIE 2007; Introduction:6593.